Molecular Therapy
Methods & Clinical Development
Original Article

Ex Vivo Gene Therapy Treats Bone Complications of Mucopolysaccharidosis Type II Mouse Models through Bone Remodeling Reactivation

Miho Wada,[1,2] Yohta Shimada,[2] Sayoko Iizuka,[2] Natsumi Ishii,[2] Hiromi Hiraki,[2] Toshiaki Tachibana,[3] Kazuhiro Maeda,[4] Mitsuru Saito,[4] Shoutaro Arakawa,[4] Takuya Ishimoto,[5] Takayoshi Nakano,[5] Hiroyuki Ida,[1,2] Toya Ohashi,[1,2] and Hiroshi Kobayashi[1,2]

[1]Department of Pediatrics, The Jikei University School of Medicine, Tokyo, Japan; [2]Division of Gene Therapy, Research Center for Medicine Sciences, The Jikei University School of Medicine, Tokyo, Japan; [3]Division of Molecular Cell Biology, Research Center for Medical Science, The Jikei University School of Medicine, Tokyo, Japan; [4]Department of Orthopaedic Surgery, The Jikei University School of Medicine, Tokyo, Japan; [5]Biomaterials & Structural Materials Design Area, Course of Materials Science & Engineering, Division of Materials & Manufacturing Science, Graduate School of Engineering, Osaka University, Osaka, Japan

Mucopolysaccharidosis type II is a disease caused by organ accumulation of glycosaminoglycans due to iduronate 2-sulfatase deficiency. This study investigated the pathophysiology of the bone complications associated with mucopolysaccharidosis II and the effect of lentivirus-mediated gene therapy of hematopoietic stem cells on bone lesions of mucopolysaccharidosis type II mouse models in comparison with enzyme replacement therapy. Bone volume, density, strength, and trabecular number were significantly higher in the untreated mucopolysaccharidosis type II mice than in wild-type mice. Accumulation of glycosaminoglycans caused reduced bone metabolism. Specifically, persistent high serum iduronate 2-sulfatase levels and release of glycosaminoglycans from osteoblasts and osteoclasts in mucopolysaccharidosis type II mice that had undergone gene therapy reactivated bone lineage remodeling, subsequently reducing bone mineral density, strength, and trabecular number to a similar degree as that observed in wild-type mice. Bone formation, resorption parameters, and mineral density in the diaphysis edge did not appear to have been affected by the irradiation administered as a pre-treatment for gene therapy. Hence, the therapeutic effect of gene therapy on the bone complications of mucopolysaccharidosis type II mice possibly outweighed that of enzyme replacement therapy in many aspects.

INTRODUCTION

Mucopolysaccharidosis type II (MPS II; Hunter syndrome) is a disease in which various organs accumulate glycosaminoglycans (GAGs) due to iduronate 2-sulfatase (IDS) deficiency. Abnormal ossification affects all skeletal bones and joints, with significant effects on daily life.[1–4] Recently, enzyme replacement therapy (ERT) and hematopoietic stem cell (HSC) transplantation (HSCT) have been introduced as treatments for MPS II. Although ERT treatment can delay disease progression,[5–7] the associated effects on the central nervous system (CNS) and bone lesions are reportedly poor.[8–11] Furthermore, secondary ineffectiveness due to the antibodies produced via long-term administration also constitutes a serious concern.[12,13]

In HSCT, transplanted donor HSCs reported ly differentiate into microglia and engraft in the brain, thereby exerting a "cross-correction" effect.[12] However, HSCT is not sufficiently effective in the CNS lesions of MPS II patients, resulting in negative reviews in the US and Europe.[14–17] We have also demonstrated that ERT and HSCT are ineffective in MPS II CNS and bone lesions.[18]

In recent years, clinical trials of HSC gene therapy using lentiviral vectors have proven effective in adrenoleukodystrophy, metachromatic leukodystrophy, Wiskott-Aldrich syndrome, and β-thalassemia.[19–22]. Furthermore, HSCs modified by gene therapy are reportedly effective in treating mouse MPS I and MPS IIIA models.[23,24] In fact, we have succeeded in improving the CNS lesions in MPS II mouse models by administering HSCs that had undergone lentivirus-mediated gene therapy.[25] We have also observed that high levels of IDS are continuously secreted into the blood due to overexpression of *IDS* in HSCs and exert beneficial effects on the CNS. Accordingly, we hypothesized that gene therapy could also improve bone lesions (Figure 1). To this end, we investigated the pathophysiologic mechanism of MPS II bone lesions by considering the factors that have not yet been examined, including osteoclasts, osteoblasts, bone mineral density, and bone strength. In addition, we performed gene therapy on HSCs using a lentiviral vector system and examined the effect of these modified HSCs on bone lesions with the aim of establishing a novel treatment for the bone complications associated with MPS II.

Received 7 February 2020; accepted 16 September 2020;
https://doi.org/10.1016/j.omtm.2020.09.012.

Correspondence: Hiroshi Kobayashi, Department of Pediatrics, The Jikei University School of Medicine, 3-5-28 Nishi-Shimbashi, Minato-ku, Tokyo, Japan.
E-mail: hrkb2012@gmail.com

This is an open access article under the CC BY-NC-ND license (http://creativecommons.org/licenses/by-nc-nd/4.0/).

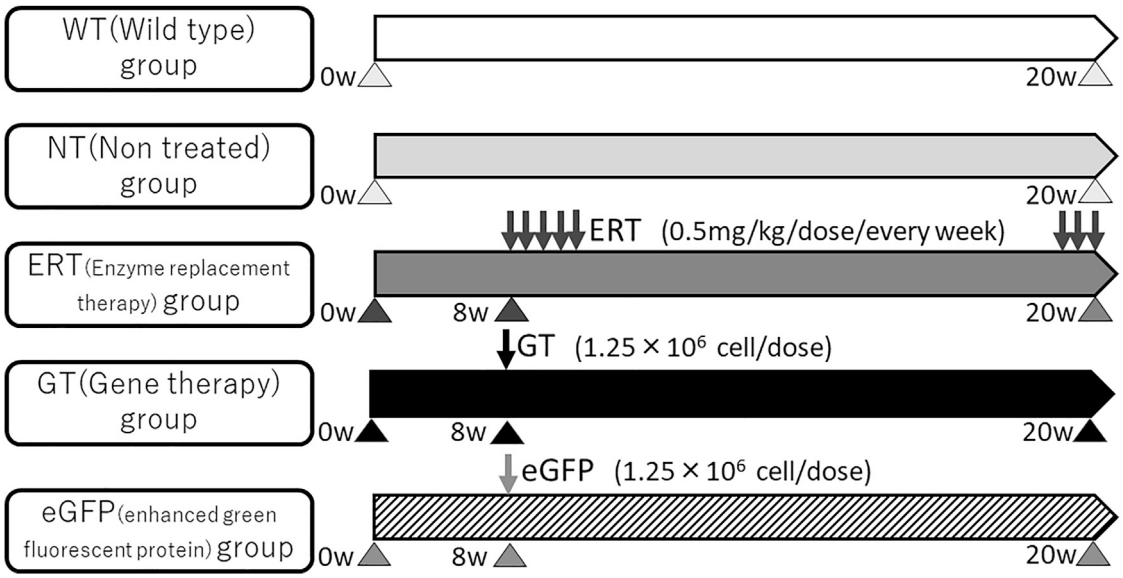

Figure 1. Treatment Protocol

Experimental design. Diagram showing the therapeutic regimen. The therapeutic groups included gene therapy (GT), enzyme replacement therapy (ERT), and enhanced green fluorescent protein (EGFP). Solid arrows indicate the initiation of GT, EGFP, or IDS administration. ERT treatment was initiated at 8 weeks of age, followed by weekly infusions, which were performed 13 times. GT and EGFP treatments were carried out at 8 weeks of age. All of the mice were sacrificed 12 weeks after treatment initiation.

RESULTS

Transplantation of Mice with HSCs Engineered to Express the Enhanced Green Fluorescent Protein (*EGFP*) Gene

EGFP expression in each lineage was evaluated in the peripheral blood of 20-week-old mice transplanted with HSCs isolated from 8-week-old mice and transfected with *EGFP*. Expression of *EGFP* was observed in 60.2% of the peripheral blood leukocytes, 79.2% of the granulocytes (Ly-6G-positive), 56.8% of the B cells (CD45R-positive), and 52.5% of the T cells (CD3-positive) (Figure 2A). Moreover, vector copy numbers (VCNs) measured in the cerebrum, liver, and spleen 12 weeks after initiating the treatments were 0.005, 0.098, and 1.131, respectively, suggesting that the transfected donor HSCs differentiated into all hematopoietic cell lineages and were detected in the peripheral blood and multiple organs (Figure 2B).

Ex Vivo Gene Therapy Caused Persistently High IDS Activity in the Serum and Organs, and a Significantly Low Substrate (GAGs) Level

IDS activity following transplantation was assessed via time-course experiments. Sustained low IDS activity was observed in untreated, control MPS II, and ERT-treated mice, compared with that in age-matched wild-type (WT) mice. In addition, a highly significant activity ($p < 0.0001$), which was approximately 17.5-fold higher than that of WT mice, was continuously observed in mice treated with gene therapy. This observation suggests that the donor cells were stably engrafted following *ex vivo* gene therapy, and persistently expressed IDS (Figure 3A).

Furthermore, 12 weeks after initiating the treatments, IDS activity of the bone, cerebrum, and liver of each group was measured. In mice treated with ERT, no significant increase in IDS activity was observed in any organs compared with that in untreated mice. The mice that received gene therapy had significantly higher IDS activity ($p < 0.0001$) in the tibia and liver than did untreated mice, with the activity being 27-fold higher in the tibia and 14-fold higher in the liver than in those of WT mice. Furthermore, the IDS activity in the tibia and liver of the gene therapy mice was also significantly higher ($p < 0.0001$) than that in ERT-treated mice. Moreover, the IDS activity in the cerebrum of gene therapy mice was only 3.2% that in WT mice, and 6.6-fold higher than that in the untreated mice (Figure 3B).

Overall, these results indicated that stable donor cell engraftment in mice receiving *ex vivo* gene therapy contributed to the increased IDS activity in various organs. Furthermore, to examine the effects of gene therapy and ERT on bone and CNS lesions, GAGs of the tibia, cerebrum, and liver were measured using liquid chromatography (LC)-mass spectrometry (MS) 12 weeks after transplantation. The GAG accumulations in the tibia and liver were significantly reduced ($p < 0.01$ and $p < 0.0001$, respectively) in the MPS II mice treated with ERT compared with those in untreated mice. Furthermore, the mice treated with gene therapy showed significantly lower GAG accumulations ($p < 0.01$ in the tibia and cerebrum; $p < 0.0001$ in the liver) in all organs than did untreated mice (Figure 3C).

Ex Vivo Gene Therapy Induced Low Bone Volume and Formation Rate, and Low Trabecular and Osteoclast Numbers

Several components of the skeletal system of the mice were analyzed 12 weeks after transplantation. Untreated mice showed significantly higher values ($p < 0.0001$) in intermaxillary width and zygomatic arch thickness than those in WT mice. Although significantly lower

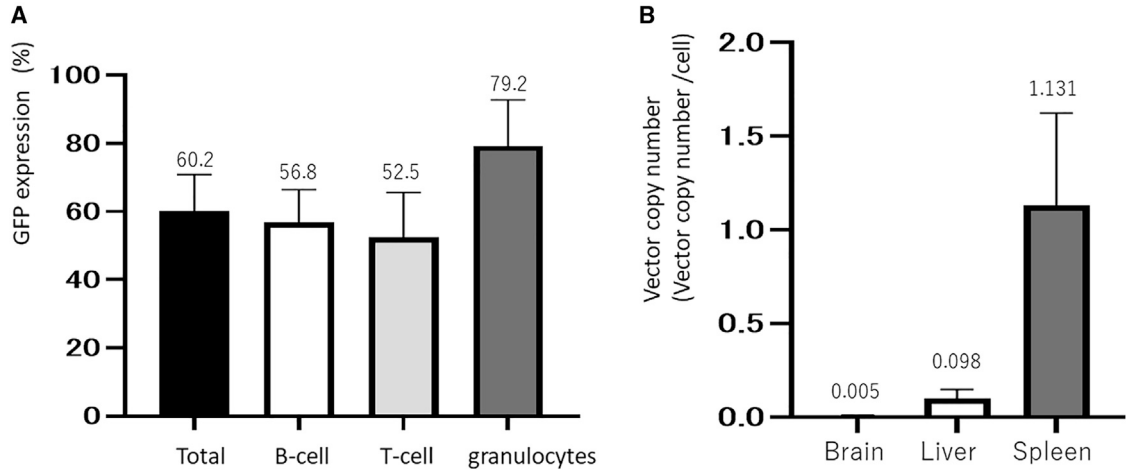

Figure 2. EGFP Expression in Peripheral Blood, and Tissue Vector Copy Number (in the GT Group)

(A) EGFP expression in peripheral blood. Graft-derived total blood cells, T cells, B cells, and granulocytes in the recipient peripheral blood were quantitated. The peripheral blood of the recipient mice was collected 12 weeks after the transplantation of EGFP-transfected HSCs and used for analysis. The expression rate of EGFP is presented as percent (mean ± SD, n = 6). (B) Tissue vector copy number (the GT group). The lentiviral copy numbers in the brain, liver, and spleen were determined by quantitative PCR 12 weeks after transplantation. The limit of detection was 0.0001 copy per cell. The vector copy number is expressed as vector copy number/cell (mean ± SD, n = 6). It was confirmed that the gene-transferred donor cells were differentiated, transferred, and expressed in each organ.

values of intermaxillary width ($p < 0.0001$) and zygomatic arch thickness ($p < 0.001$) were observed in mice treated with ERT than in untreated mice, the values in the mice treated with gene therapy were much lower ($p < 0.0001$ for both intermaxillary width and zygomatic arch thickness). In addition, mice transplanted with *EGFP*-transfected HSCs instead of *IDS*-transfected HSCs had similar values as untreated mice. These results indicated that radiation had no effect on the skull measurements of MPS II mice treated with gene therapy, and that the therapeutic effect of gene therapy was more significant than that of ERT (Figure 4).

Next, the histopathology of the bone was studied using the tibia of mice 12 weeks after initiating the treatments. The bone volume and trabecular number in the untreated mice were significantly higher than those in WT mice. MPS II mice treated with gene therapy exhibited significantly lower bone volume and trabecular number ($p < 0.01$ and $p < 0.0001$, respectively) than did untreated mice, unlike those treated with ERT. However, the bone volume and trabecular number of *EGFP*-transfected mice were also significantly lower than those of untreated mice ($p < 0.01$ and $p < 0.001$, respectively), suggesting an irradiation effect for these factors. The trabecular number was significantly higher ($p < 0.01$) in mice treated with ERT than in mice treated with gene therapy (Figures 5A and 5B).

Bone resorption and formation parameters were compared next. The osteoclast number of the mice treated with gene therapy was significantly greater ($p < 0.001$) than that of untreated mice, suggesting that bone resorption was activated by gene therapy. The bone formation rate in mice treated with gene therapy was significantly higher ($p < 0.05$) than that in untreated mice, suggesting that bone formation was also activated by gene therapy. There was no significant increase in either parameter in mice treated with ERT compared with those in untreated mice. Furthermore, the osteoclast number and bone formation rate were respectively higher and lower in the *EGFP*-transfected mice with irradiation than in WT and untreated mice (Figures 5C and 5D).

We also performed fluorescent staining of tibia and confirmed that more bone formation occurred in the mice treated with gene therapy and WT mice due to the longer distance between the front lines of the calcification labeled with fluorescence at the calcein administration interval (Figure S1). Furthermore, the number of osteoclasts was increased in the mice treated with gene therapy as observed by tartrate-resistant acid phosphatase (TRAP) staining, which is specific for osteoclasts (Figure S2).

Ex Vivo Gene Therapy Resulted in Low Bone Mineral Density, Low Bone Strength, and Loss of Vacuolation in Osteocytes, Osteoblasts, and Osteoclasts

Femoral bone mineral density in the diaphysis and diaphysis edge was significantly higher in untreated mice than in WT mice ($p < 0.05$) but it was significantly lower in mice treated with gene therapy than in untreated mice ($p < 0.001$ and $p < 0.0001$ for both the diaphysis and diaphysis edge).

Bone mineral densities in the diaphysis and diaphysis edge of the mice treated with ERT were not significantly lower than those in untreated mice. Moreover, although bone mineral density in the diaphysis of the *EGFP*-transfected mice was significantly lower ($p < 0.01$) than that of untreated mice, the bone mineral density in the diaphysis edge was not (Figure 6A).

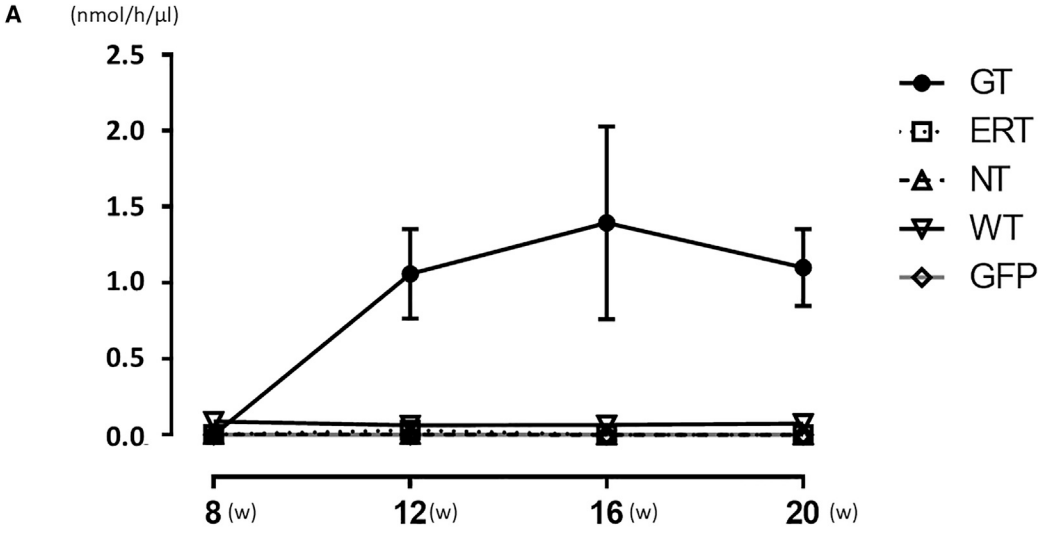

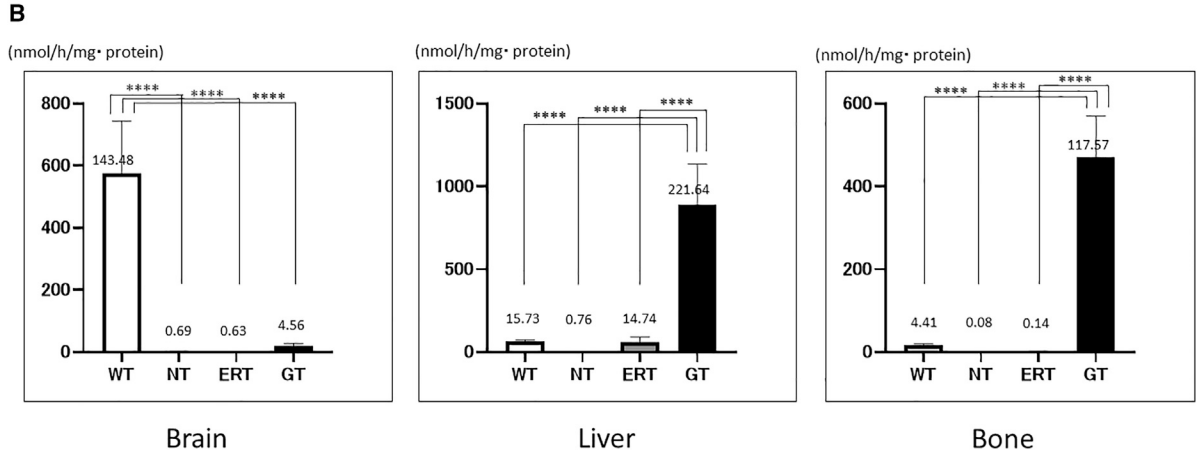

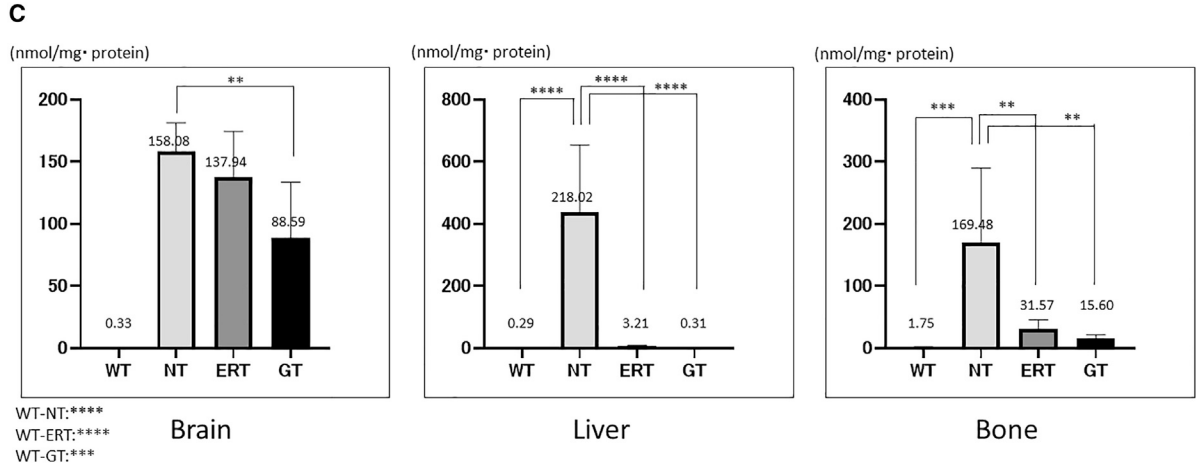

(legend on next page)

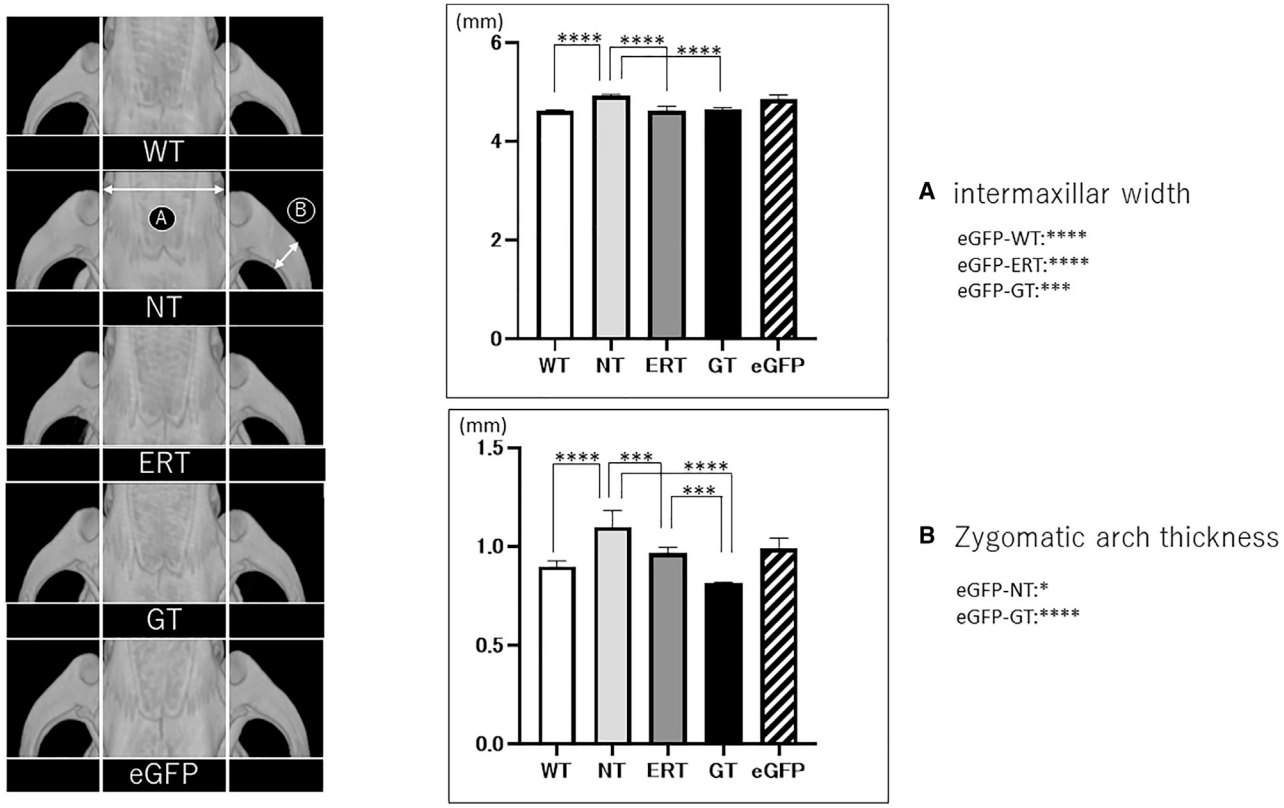

Figure 4. Skull Measurement by Micro-CT Scan

Skull measurements obtained from WT, NT, ERT, GT, and EGFP mice 12 weeks after initiating the treatments. (A and B) The maximum diameter of the width of the intermaxillary (A) and the thickness of the zygomatic bone (B) at the forehead were measured using CT scans. Although significantly lower values of intermaxillary width and zygomatic arch thickness were observed in ERT mice than in NT mice, the values in GT mice were much lower. Skull measurement is expressed in mm (mean ± SD, n = 5–6). Statistical analyses of the data were performed by one-way analysis of variance (Bonferroni post-test). *$p < 0.05$, **$p < 0.01$, ***$p < 0.001$, ****$p < 0.0001$.

We also measured bone surface, bone mineral density, and bone mineral content in the skull and femur by micro-computed tomography (micro-CT) analysis. Total bone surface in the skull of mice treated with gene therapy was significantly lower than that of untreated mice ($p < 0.01$) and mice treated with ERT ($p < 0.05$). Total bone mineral density in the femur of mice treated with ERT and gene therapy was significantly lower than that of untreated mice ($p < 0.05$, $p < 0.01$), and total bone mineral content in the femur of mice treated with gene therapy was significantly lower ($p < 0.01$) than that of untreated mice. A low value was also observed in mice treated with ERT; however, there was no significant difference. Furthermore, total bone mineral content in the skull of mice treated with gene therapy and ERT was significantly lower than that of untreated mice ($p < 0.0001$), and this tendency was the same as that observed in WT mice (Figure S3).

A bone strength test was performed using femurs 12 weeks after transplantation. Breaking energy measured via the three-point bending test was significantly higher ($p < 0.0001$) in untreated mice than in WT mice but was significantly lower in mice treated with ERT than in untreated mice ($p < 0.05$), and significantly lower breaking energy values were also observed in mice treated with gene therapy ($p < 0.0001$). In addition, breaking energy values of

Figure 3. Serum IDS Activity (Tissue IDS Activity and Tissue GAGs)

(A) Serum IDS activity. Serum was collected from WT, MPS II (NT), ERT, and GT mice every 4 weeks after treatment. In the GT mice, a significant activity, approximately 17.5-fold higher than that of WT mice, was continuously observed. IDS activities are expressed as nmol/h/μL serum (mean ± SD, n = 5–7). (B) Tissue IDS activity. Brain, liver, and bone tissues were obtained from WT, NT, ERT, and GT mice 12 weeks after initiating the treatments. Significantly higher IDS activity was observed in the tibia and liver in GT mice than in NT mice, and cerebral IDS activity was higher in GT mice than in NT mice, although the difference was not significant. The IDS activity in each tissue is in nmol/h/mg protein (mean ± SD, n = 6). Statistical analyses of the data were performed by one-way analysis of variance (Bonferroni post-test). ****$p < 0.0001$. (C) Tissue GAGs. GAGs in the brain, liver, and bone derived from WT, NT, ERT, and GT mice were measured using liquid chromatography-tandem mass spectrometry (LC-MS/MS) as described in Materials and Methods. The GAG accumulations in the bone and liver of the ERT and GT mice, and in the brain of the GT mice, were significantly lower compared to those of the NT mice. The amounts of GAGs are presented in nmol/mg protein (mean ± SD, n = 6). Statistical analyses of the data were performed by one-way analysis of variance (Bonferroni post-test).**$p < 0.01$, ***$p < 0.001$, ****$p < 0.0001$.

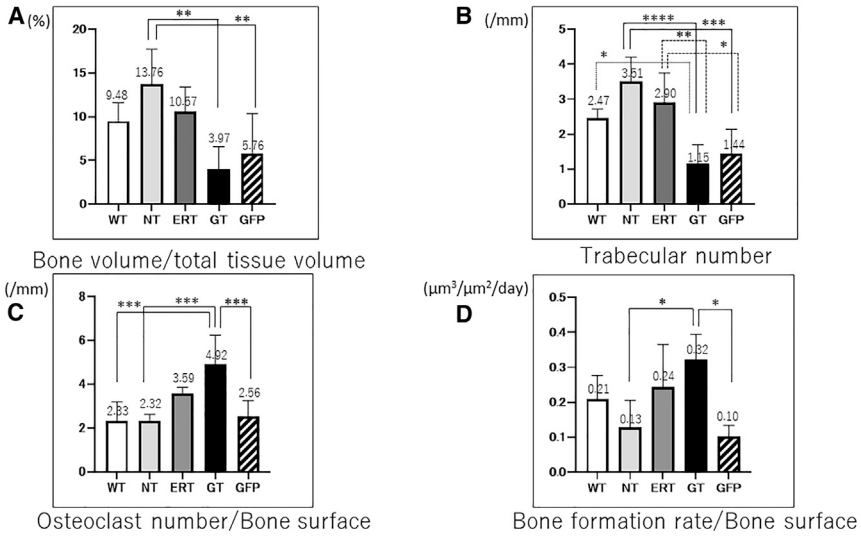

Figure 5. Histopathology (Tibia)

Histopathological results obtained from WT, NT, ERT, GT, and EGFP mice 12 weeks after initiating treatments. (A–D) The bone volume (A), trabecular number (B), osteoclast number (C), and bone formation rate (D) were measured using OsteoMeasure (mean ± SD, n = 4–6). The bone volume and trabecular number of the GT mice were significantly lower than those of the NT mice. The osteoclast number of GT mice was significantly higher than that of NT mice. The bone formation rate of GT mice was significantly higher than that of NT mice. Statistical analyses of the data were performed by one-way analysis of variance (Bonferroni post-test). *p < 0.05, **p < 0.01, ***p < 0.001, ****p < 0.0001.

EGFP-transfected mice were significantly lower ($p < 0.01$) than those of untreated mice. There was no significant difference between WT mice and untreated mice regarding the maximum load and stiffness (Figure 6B).

To examine differences in natural history as well as the effects of gene therapy between WT mice and untreated mice, we measured apatite content in the femur 12 weeks following treatment initiation. There was no significant difference among WT, untreated, gene therapy-treated, and *EGFP*-transfected mice (Figure 6C).

To examine the difference between the effects of gene therapy and ERT, the femurs of mice at 12 weeks following treatment initiation were compared using Alcian blue staining and electron microscopy. Alcian blue staining showed intense blue staining, which reflects GAG accumulation, in untreated mice relative to that in WT mice. Although ERT treatment decreased the intensity of the staining, indicating a reduction in GAG amount, the gene therapy decreased the intensity much more than ERT (Figure 7). Furthermore, *EGFP*-transfected mice showed equally intense Alcian blue staining as untreated mice.

Vacuolation in osteocytes reflects GAG accumulation, and electron microscopy analysis revealed that mice treated with ERT had reduced vacuolation relative to that in untreated mice. Importantly, such vacuolation was not evident in the mice treated with gene therapy (Figure 8A). Similar results were obtained for osteoblasts and osteoclasts (Figures 8B and 8C). These results suggested that stable donor cell engraftment via *ex vivo* gene therapy contributed to efficient GAG reduction in osteocytes, osteoblasts, and osteoclasts of MPS II mice.

DISCUSSION

The pathophysiological mechanism of bone lesions observed in MPS type II is not fully understood. MPS type I, III, and VII mouse models reportedly exhibit high bone mineral density and GAG accumulation compared with WT mice.[26–29] Some reports have indicated that these counts tend to improve in mouse models subjected to ERT and HSCT combination therapy, neonatal HSCT, and gene therapy. Although skeletal changes have been reported in behavioral analyses, as well as in X-ray and CT images, of MPS II mouse models,[30–32] studies comparing histopathology, bone mineral densitometry, and disease-specific GAG measurements are scarce. Herein, we confirmed the effect of HSC gene therapy on bone lesions. Lentivirus-based HSC gene therapy revealed IDS activity not only in the cerebrum and liver, but also in the bone, and high lentiviral vector copy numbers were observed in the cerebrum, liver, and spleen of the recipient mice. In our previous study, high lentiviral vector copy numbers were observed in the cerebrum of mice treated with HSC gene therapy, in which the transplanted HSCs differentiated into microglia via the process of transitioning to the central nerve. Cross-correction effects resulted in the improvement of CNS lesions in MPS II mouse models.[25] The results of this study indicated that *ex vivo* gene therapy might improve bone lesions via differentiation of transfected HSCs or cross-correction effects caused by the high IDS level in the blood of MPS II mice.

In addition, IDS activity in the serum of mice treated with *ex vivo* gene therapy was approximately 17.5-fold higher than that in the serum of WT mice. Previous studies demonstrated that IDS activity in the serum of MPS II mice treated with adeno-associated virus (AAV)-mediated gene therapy was approximately 5-fold higher than that of WT mice, resulting in improved CNS and bone lesions.[31,33] In this study, serum IDS activity was high enough to exert similar effects. These results suggest that donor cells were stably engrafted following transplantation and that the persistent expression of IDS in various organs and serum resulted in a significant reduction in disease-specific GAGs in the bone. A previous study evaluating the presence or absence of antibody production against IDS reported a very small expression of anti-IDS antibody under ERT.[18] Furthermore, a previous study reported that antibody production for gene therapy by

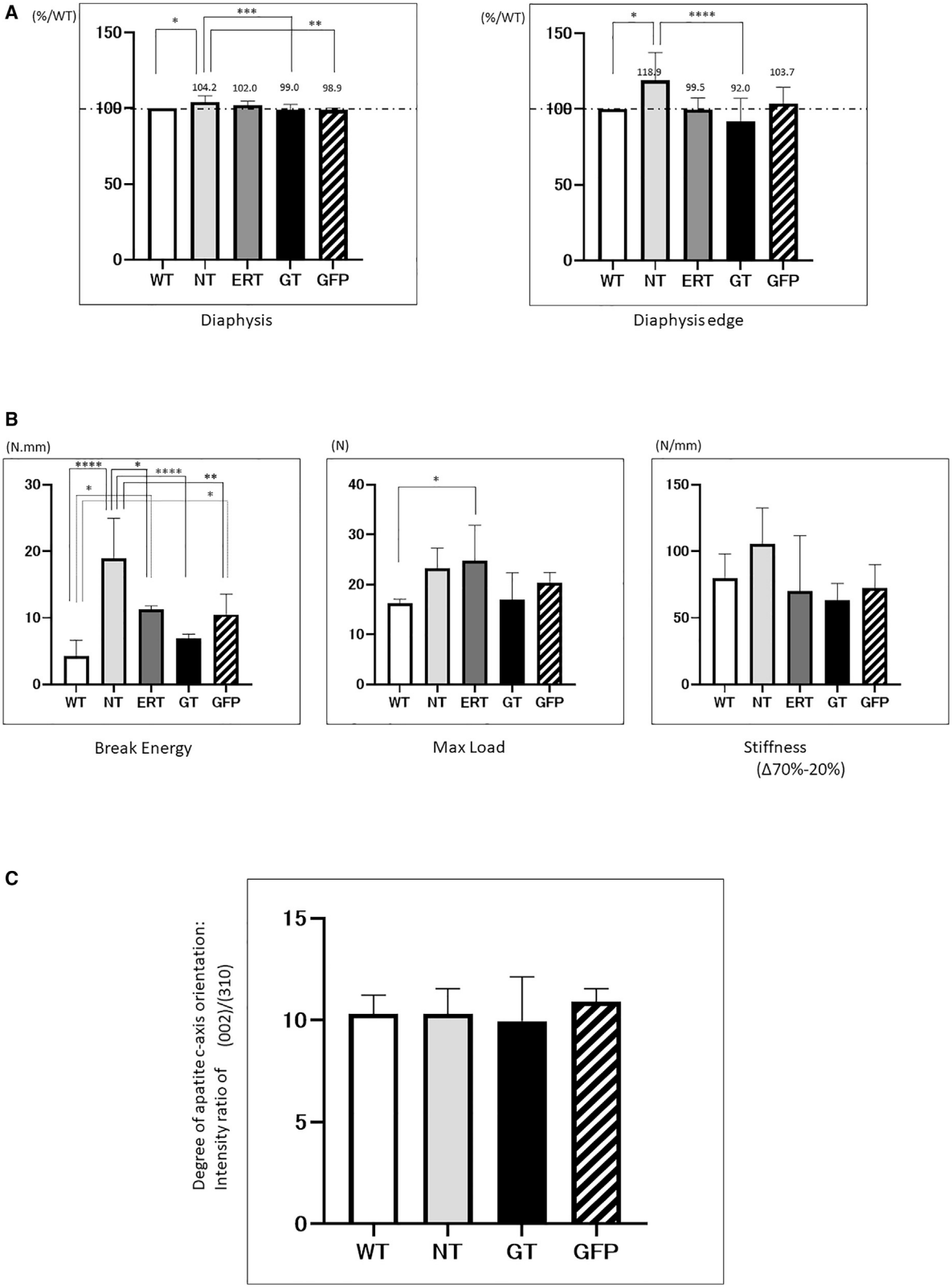

(legend on next page)

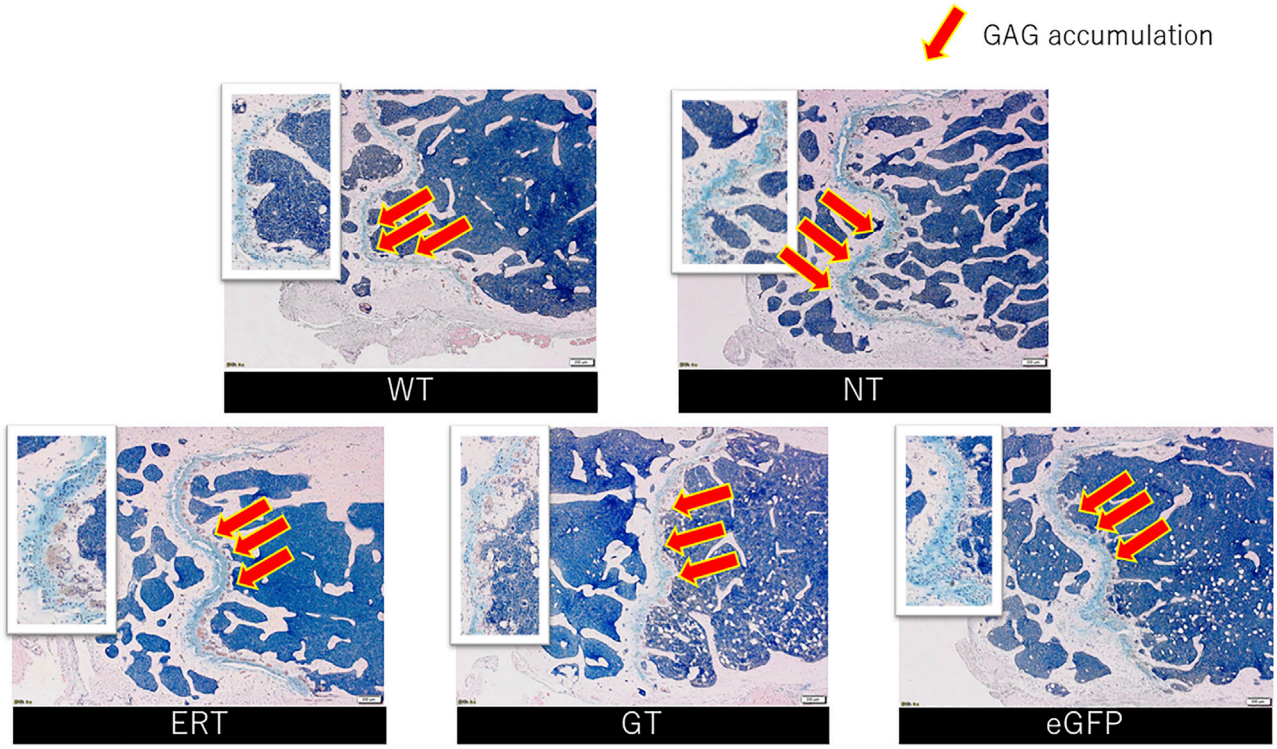

Figure 7. Alcian Blue Staining

Alcian blue-stained images of the femurs from WT, NT, ERT, GT, and EGPF mice 12 weeks after initiating the treatments. Red arrows indicate GAG accumulation as light blue region. The intensity of the light blue color is proportional to the amount of GAG. We detected lower intensity of the light blue color in GT mice compared to NT and EGFP mice.

lentivirus was in the normal range.[34] Therefore, it is unlikely that antibody affects the therapeutic effect.

Histological evaluation has indicated that gene therapy with AAV enhances the accumulation of substances in various organs other than bone in MPS II mouse models,[35] substantiating previous reports. Moreover, another study has demonstrated that accumulated substances in osteocytes, osteoblasts, and osteoclasts are reduced via HSC transplantation in MPS I mouse models.[27] Additionally, the current study reported that vacuolation, which is present in osteoblasts and osteoclasts in untreated mice, tended to be reduced in mice treated with ERT and appeared to be absent in mice treated with gene therapy. This observation indicated that accumulated substances, such as GAGs, decreased in both treatment groups. The decrease of accumulated substances in mice treated with gene therapy, compared with those treated with ERT, may be due to the persistently high IDS levels. These tendencies were also reflected in the skull measurements.

In histopathological analyses, the increase in bone volume and trabecular number was significantly lower in mice treated with gene therapy than in the untreated mice. However, the bone volume and trabecular number were significantly lower even in the group subjected to radiation pre-treatment followed by *EGFP* treatment instead of IDS. This observation suggests that the results of gene therapy might have been affected by radiation. However, these values were also low in

Figure 6. Femur Bone Mineral Density and Strength Measurements and Biological Apatite

(A) Femur bone mineral density measurement. The bone mineral densities of WT, NT, ERT, GT, and EGFP mice 12 weeks after initiating the treatments. Bone mineral densities in the diaphysis and diaphysis edge were measured using pQCT. Bone mineral density is expressed as the percentage of WT (%/WT) (mean ± SD, n = 4–12). Femoral bone mineral density in the diaphysis and diaphysis edge was significantly lower in GT mice than in NT mice. Statistical analyses of the data were performed by one-way analysis of variance (Bonferroni post-test). *$p < 0.05$, **$p < 0.01$, ***$p < 0.001$, ****$p < 0.0001$. (B) Femur bone strength measurement. The bone strength of WT, NT, ERT, GT, and EGFP mice 12 weeks after initiating the treatments. The break energy, maximum load, and stiffness, as the three points of bending tests, were measured using the MZ-500S (mean ± SD, n = 4–6). Breaking energy values were significantly lower in GT mice than in NT mice. Statistical analyses of the data were performed by one-way analysis of variance (Bonferroni post-test). *$p < 0.05$, **$p < 0.01$, ***$p < 0.001$, ****$p < 0.0001$. (C) Biological apatite. Biological apatite of WT, NT, GT, and EGFP mice 12 weeks after initiating the treatments. The c-axis orientation of apatite was analyzed by microbeam X-ray analysis. The biological apatite is expressed as intensity ratio of (002)/(310) (mean ± SD, n = 6). There was no significant difference among WT, NT, GT, and EGFP mice. Statistical analyses of the data were performed by one-way analysis of variance (Bonferroni post-test). *$p < 0.05$, **$p < 0.01$, ***$p < 0.001$, ****$p < 0.0001$.

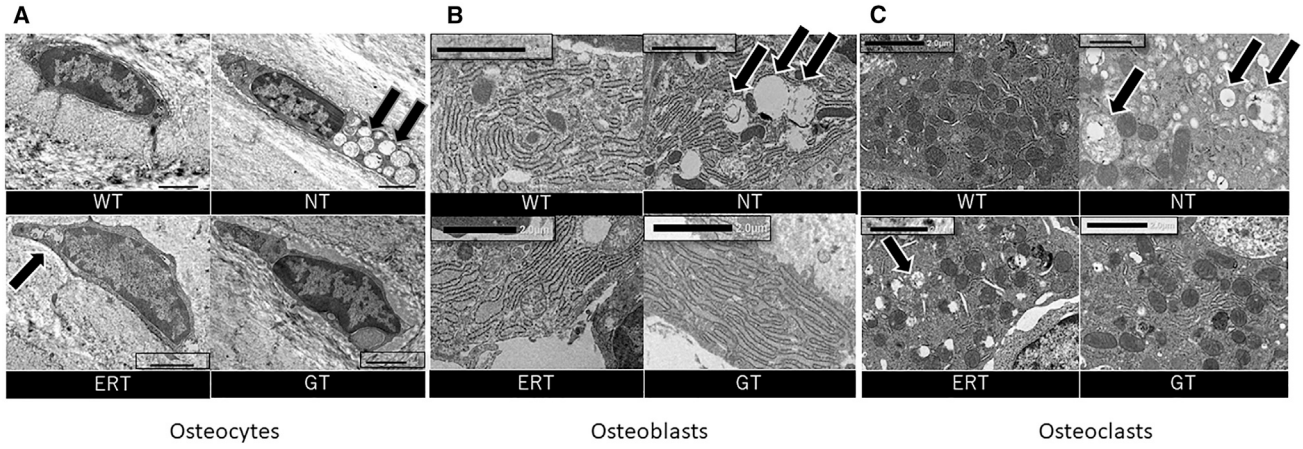

Figure 8. Electron Micrograph of the Femur

Electron microscopy images of the femurs from WT, NT, ERT, and GT mice 12 weeks after initiating the treatments. (A–C) Electron microscopy images of the osteocytes (A), osteoblasts (B), and osteoclasts (C) were observed using a transmission electron microscope. Black arrows indicate vacuolation. We detected no vacuolation in GT and WT mice and reduction of vacuolation in ERT mice relative to NT mice in the osteocyte, osteoblast, and osteoclasts.

the ERT-treated mice, which did not undergo radiation. Similar results have been reported for measurements obtained via micro-CT in HSC gene therapy for MPS VII mice under conditions in which no pre-treatment was administered.[29,36,37] Therefore, although the effect of radiation needs to be taken into consideration, the reduction in bone volume and trabecular number was presumably due to the effect of GAG reduction induced by the gene therapy. Furthermore, this study observed that both bone resorption (osteoclast number) and bone formation (bone formation rate) tended to be lower in untreated mice than in WT mice, indicating that bone metabolism was reduced in MPS II mice. In addition, *ex vivo* gene therapy reactivates bone resorption and formation, with the former being primarily activated, resulting in reduced bone volume and trabecular number. Osteoclasts are specialized cells responsible for bone resorption. They develop from macrophage-derived cells under the control of osteoblasts and osteocytes (osteoblast-lineage cells). Osteoblast-lineage cells express receptor activator of nuclear factor κB (NF-κB) ligand (RANKL) essential for osteoclast differentiation. They also express osteoprotegerin (OPG), which is a decoy receptor of RANKL, and suppress osteoclastogenesis. Recent findings suggest that the binding of dermatan sulfate induced by gene therapy to the osteoclast inhibitor, OPG, causes excessive bone resorption due to a relative increase in RANKL, thus substantiating the promotion of bone resorption in this study.[27,38–40] Additionally, although no study has used the same method utilized in the current study for the quantitation of the number of osteoclasts, similar tendencies in MPS VII mice have been reported when analyzed via osteoclast culture.[29] In the EGFP-treated mouse group showing radiation effects, osteoclast number tended to be slightly higher and bone formation rate tended to be lower than those in WT mice and untreated mice. In other studies, irradiation in C57BL/6 mice induced bone loss, osteoclast activation, osteocyte apoptosis, and osteoblast proliferation impairment.[41,42] The results of our study indicated that *ex vivo* gene therapy induced not only osteoclast activation but also osteoblast activation and increasing bone formation rate, suggesting that osteoblast proliferation exceeded osteocyte apoptosis.

Bone mineral densities in the diaphysis as well as in the diaphysis edge were significantly high in untreated mice compared with those in WT mice. In mice treated with gene therapy, bone mineral density was significantly lower than that in untreated mice, suggesting similar trends to those observed in WT mice. In addition, analyses of *EGFP*-transfected mice showed radiation effects, suggesting that radiation affected bone mineral density in the diaphysis but not in the diaphysis edge in this study.

In the micro-CT analysis of the skull and femur, differences were observed in the therapeutic effect and radiation effect depending on the site. The bone surface and bone mineral content in the skull, as well as the bone mineral density in the femur, were significantly lower in mice treated with gene therapy than in untreated mice. Although the effects of radiation were also taken into consideration in each case, it is considered that the treatment contributed the largest effect, as ERT mice also exhibited a significant decrease. The results of evaluation of the skull also reflected the slimming of the zygomatic bone and narrowing of the intermaxillary width, as shown in Figure 4, and the results of evaluation of the femur were in agreement with the peripheral quantitative CT (pQCT) analysis results in Figure 6A. A previous study reported skeletal improvement in gene therapy by lentivirus in MPS II mice,[34] consistent with this study.

Furthermore, bone quality encompasses both the structural and material properties of the bone. Apatite orientation is an important factor when considering the material properties of bone tissue. The degree of apatite orientation is an important indicator of nanoscale microstructure, associated mechanical function, and bone disease.[43]

Thus, apatite orientation represents the material properties of the bone tissue. Apatite orientation is considered to depend on collagen orientation,[44] and deterioration of biological apatite leads to abnormalities in collagen, thereby weakening bone strength.[45,46] The current study did not detect any significant difference in biological apatite among the tested groups, suggesting that the effects of these factors were low.

The break energy in the bone strength tests was significantly high in untreated mice compared with that in WT mice, indicating that bone strength trends in mice treated with gene therapy were similar to those in WT mice. These results indicate that bone strength consists of two factors, bone mineral density and bone tissue material properties.[47]

In summary, in MPS II the accumulation of GAGs in the bone reduces bone metabolism and increases trabecular number, resulting in an increase in bone mineral density and strength. Consistently high serum IDS levels, together with the release of GAGs from osteoblasts and osteoclasts, resulted in the reactivation of bone metabolism as detected in mice treated with gene therapy. Simultaneously, as the balance shifted toward osteoclasts, the number of trabeculae decreased, resulting in decreased bone mineral density and bone strength to a similar degree as in WT mice.

These results revealed the mechanism by which lentiviral vector-mediated gene therapy targeting HSCs allows enzymes to reach bone lineages, leading to a reduction or elimination of GAGs, whereby actual bone lineage remodeling is reactivated. These processes were made possible by continuously maintaining the enzyme activity at several times higher than that provided by ERT, and based on the evaluation, the efficacy of gene therapy is still apparent even when considering the effects of radiation.

In conclusion, it is suggested that gene therapy targeting HSCs is an effective treatment option for the bone lesions in MPS II and may also be applicable to other types of MPS displaying a high degree of bone pathology, such as Morquio syndrome.

MATERIALS AND METHODS

MPS II Mouse Model

A female heterozygous mouse, with *IDS* knockout on the X chromosome, was obtained from Dr. Joseph Muenzer (University of North Carolina)[30] and crossed with male WT (C57BL/6) mice to generate *IDS* knockout male mice (B6N.Cg-*Ids*^{tm1Muen}/J). Tail tips were collected from the male offspring $\leq$7 weeks old and used for genotyping by PCR to identify the hemi mice (IDS knockout mice: MPS II mice).[18] The mice were housed in pairs at 24°C under a 12-h light/12-h dark cycle. The selected mice were fed a standard diet (CE-2; CLEA Japan, Japan; calcium, 1.15%; phosphorus, 1.08%). The animals were bred and treated according to the regulations and with the approval of the Genetic Recombination Experiment Committee, Pathogen Safety Committee, and Animal Experiment Committee of The Jikei Medical University (Tokyo, Japan).

Lentiviral Vector

Codon-optimized *IDS* cDNA or *EGFP* was incorporated into the second-generation lentiviral vector pSMPUR-MCU3-MCS (kindly provided by Dr. Donald B. Kohn, University of California, Los Angeles[48]), and a recombinant virus was produced using a previously described conventional method.[48] The promoter used was an enhancer of retroviral origin from a myeloproliferative sarcoma virus. This promoter generates strong and ubiquitous expression in systemic organs.[48] Virus preparation was performed according to a previously described procedure.[48] All treatments, including virus purification, were approved by The Jikei University School of Medicine (Tokyo, Japan) Genetic Recombination Experiment Committee and the Pathogen Safety Committee.

HSCT

Bone marrow cells were collected from the femurs and tibias of 8-week-old MPS II mice, and lineage-negative cells were collected using a lineage cell depletion kit (Miltenyi Biotec, Auburn, CA, USA), which is a system that effectively depletes mature hematopoietic cells, such as T cells, B cells, monocytes/macrophages, granulocytes, and erythrocytes, as well as their committed precursors, from bone marrow. Depletion occurs via magnetic labeling of cells with a cocktail of biotinylated antibodies against a panel of "lineage" antigens (CD5, CD45R [B220], CD11b, anti-Gr-1 [Ly6G/C], 7-4, and Ter-119 antibodies) and anti-biotin MicroBeads. This labeling effectively leaves lineage-negative cells untouched in the bone marrow. Next, Dulbecco's modified Eagle's medium supplemented with 10% fetal bovine serum was mixed with recombinant murine *fms*-related tyrosine kinase 3 ligand (rmFlt-3L) (100 ng/mL) (R&D Systems, Minneapolis, MN, USA), recombinant murine stem cell factor (rmSCF) (100 ng/mL) (R&D Systems), and Polybrene (8 μg/mL) (Sigma-Aldrich, St. Louis, MO, USA) and added to a RetroNectin-coated culture dish (Takara Bio, Shiga, Japan) with 1.25×10^6 lineage-negative cells.[49] Next, *IDS*- or *EGFP*-introduced lentiviral vector was used to infect the cells with a multiplicity of infection of 50. After 16 h, the virus in the culture solution was washed off twice with phosphate-buffered saline to recover the cells. Recipient MPS II mice (8 weeks old) were given a total body irradiation of 9 Gy (Hitachi MBR-1520-R irradiator) 2 h before transplantation.[18] Subsequently, they were transplanted with 1.25×10^6 infected lineage-negative cells through tail vein injections (n = 12). Enzyme activity in the serum was measured every 4 weeks following treatment, and the mice were euthanized 12 weeks after treatment. The enzyme activities of the serum, brain, liver, spleen, and bone, as well as the levels of the substrate GAGs, were measured. Bone evaluation, including histopathology analyses and bone strength measurements, was conducted.

ERT

Human IDS (Elaprase; Shire Human Genetic Therapies, USA) was administered at a dose of 0.5 mg/kg via the tail vein to 8-week-old MPS II mice. The dose was in accordance with the therapeutic dose for humans. Human IDS was provided by Sanofi Genzyme (Tokyo, Japan).

Treatment Plan

The treatment plan is shown in Figure 1.

The treatment groups were the ERT and gene therapy groups. Untreated MPS II mice (NT group), WT mice (WT group), and *EGFP*-administered mice (EGFP group) were used as controls. In the ERT group, ERT was initiated at 8 weeks of age, and IDS was administered a total of 13 times. In the gene therapy group, gene therapy was performed at 8 weeks of age. The weights of all of the mice were measured, and blood samples were collected over time. In the ERT group, a blood sample was always collected immediately before the start of ERT. At 20 weeks of age, all mice were sacrificed, and tissues were collected for biochemical and pathological analyses.

IDS Activity Measurement

The brain and liver from each animal were shredded with a homogenizer (Hiscotron; Microtec Nition, Japan), and bones were shredded using a multi-bead shocker (Yasui Kikai, Japan). All tissues were homogenized with distilled water. The protein concentrations of the collected serum and whole tibial bone/cerebral/hepatic homogenates were measured using a bicinchoninic acid (BCA) protein assay kit (Thermo Fisher Scientific, Rockford, IL, USA). The 4MU substrate (artificial substrate 4-methylumbelliferyl-α-L-iduronide 2-sulfate; Moscerdam Substrates, Rotterdam, the Netherlands) was allowed to react with the above samples according to the manufacturer's instructions. Next, IDS enzyme activity was measured using a RF5300PC spectrofluorimeter (Shimadzu, Kyoto, Japan).[50] The enzyme activity measured was expressed as nmol/h/mg protein.

Measurement of GAG levels

The tibia, cerebrum, and liver were isolated from 20-week-old mice. Their GAG levels were measured using LC-tandem MS (LC-MS/MS), which is an improved version of the disease-specific GAG measurement method,[51,52] based on the analysis of levels of 2-sulfoiduronic acid derived from the nonreducing terminal end of polysaccharides.

Flow Cytometry

The engraftment rate was analyzed using bone marrow-derived HSCs transfected with *EGFP*. The peripheral blood of the recipient mice was collected 12 weeks after transplantation, and erythrocytes were lysed using a hemolysis buffer. Next, the obtained leukocytes were allowed to react with anti-CD16/32 antibodies as a Fc blocker; Ly-6G-phycoerythrin (PE) (clone RB6-8C5), which labels granulocytes; CD45R-PE (clone RA3-B), which labels B cells; and CD3e-PE (clone 145-2C11), which labels T cells.[53] All antibodies were obtained from eBioscience (San Diego, CA, USA). The analysis was performed using a MACSQuant analyzer (Miltenyi Biotec, Bergisch Gladbach, Germany), and the expression rate of EGFP in each blood cell type was analyzed using MACSQuantify version 2.5 (Miltenyi Biotec, Bergisch Gladbach, Germany).

Quantitative PCR

Quantitative PCR was performed with a lentiviral vector (LV-IDS) packaging sequence using a 7300 real-time PCR system (Applied Biosystems, CA, USA) to measure the VCN in the cerebrum, liver, and spleen as previously described.[54]

Skull/Femur Measurement

The skull and femur were excised from 20-week-old mice and scanned with a Latheta LCT-200 (Hitachi Aloka Medical, Japan). Three-dimensional images were then constructed using VGSTUDIO MAX 2.0 software (Volume Graphics, Germany). The bone surface, bone mineral density, and bone mineral content were also measured for whole bones. In the skull, the maximum diameter of the intermaxillary width and the thickness of the zygomatic bone at the forehead were measured. The measurement site was determined as previously described.[55]

Histopathology

The bone formation marker calcein was intraperitoneally administered to 20-week-old mice 4 or 2 d before euthanasia to label the mineralizing bone. Euthanasia was performed under anesthesia, and the tibias were removed. Next, undecalcified toluidine blue-stained specimens embedded in glycol methanlacrylate acrylic (GMA) resin were viewed under a microscope to distinguish mineralized bone, osteoid, cancellous bone, osteoblasts, and osteoclasts. The area from the standard to the distal direction (1.125 mm) excluding an area of approximately 0.15–0.35 mm from the tibial proximal growth plate cartilage was defined as the secondary cancellous bone surface and observed. The area, length, distance, and number of each tissue (primary parameters) were measured using OsteoMeasure (OsteoMetrics, USA).[56] Bone volume, trabecular number, osteoclast number, and bone formation rate were calculated using the measured primary parameters.

Bone Mineral Density Measurement

The femurs of 20-week-old mice were removed, and the bone mineral density was measured using the pQCT method (XCT-Research SA+; Stratec Medizintechnik, Germany).[57,58] The femurs were then placed into a measuring container, and the diaphysis (center) and distal metaphysis were sliced (position approximately 1.2 mm in the proximal direction from the distal growth plate) at pixel dimensions of 0.12 × 0.12 mm and thickness of 0.77 mm. The volumetric cortical bone mineral density, cancellous bone mineral density, periosteal circumference, endocortical circumference, and strength strain index (SSI) were analyzed using the pQCT software, rev. 6.00B. The cortical region was determined with a threshold value of 690 mg/cm^3, and SSI was analyzed at a threshold of 464 mg/cm^3.

Bone Strength Test

The femurs of 20-week-old mice were removed, and a three-point bending test of the femoral diaphysis was conducted using a bone strength measuring device (MZ-500S; Maruto, Japan) and a bone strength inspection system (CTRwin version 1.05; System Supply, Japan).[57,58] The specimen was placed on the sample stand with a 6-mm distance between the fulcrums, and the fracture test was performed at a fracture rate of 5 mm/min from above approximately the central portion of the diaphysis. The load cell used was 500

kilogram-force (kgf). Breaking time (s), axial displacement (mm), breaking load (kgf), maximum load (kgf), and chart area (mm^2) were calculated as the primary parameters. The fracture energy (Nm), maximum load (N), and stiffness (N/mm) were obtained as secondary parameters via automatic calculation with software.

Biological Apatite

The femurs of 20-week-old mice were removed, and the c-axis orientation of apatite was evaluated via microbeam X-ray analysis. The degree of apatite orientation in the longitudinal direction of the bone was measured at femur mid-diaphysis, and R-Axis BQ (Rigaku, Japan) was used as the analyzer.[59] The analysis method was in accordance with a previously published report.[59]

Histological Analysis of Femurs

The femurs of 20-week-old mice were excised, decalcified with ethylenediaminetetraacetate (EDTA), and embedded in paraffin without shaping. Sections of 4-μm thickness were prepared from one specimen. Afterward, the sections were dehydrated in an alcohol rising column followed by successive immersion in xylene and paraffin. Alcohol immersion was performed for approximately 10 min, and xylene immersion was performed for approximately 40 min (20 min for para-xylene removal and approximately 20 min for alcohol removal). The samples were stained with Alcian blue and observed using a system microscope (BX53 biological microscope; Olympus, Japan).

Femur Electron Microscopy

The femurs of 20-week-old mice were isolated, immersed in 2% paraformaldehyde and 2.5% glutaraldehyde, adjusted with 0.1 M phosphate buffer, and pre-fixed at 4°C for 3 days. After washing the pre-fix with 0.1 M phosphate buffer, post-fixation was carried out for 2 h with 1% osmic acid. Sample dehydration was performed using ethanol gradients of 50%, 70%, 80%, and 90% at 4°C, followed by 100% ethanol at room temperature. Samples were then embedded in epoxy resin (Epok 812; Oken, Japan) through propylene oxide. Approximately 80-nm ultrathin sections sliced with a diamond knife were electron-stained using uranyl acetate and lead citrate. Next, osteocytes, osteoblasts, and osteoclasts were observed under a transmission electron microscope (JEM 1400 Plus; JEOL, Japan).

Statistical Analysis

Statistical analyses were performed using GraphPad Prism software (GraphPad). A Student's t test or one-way analysis of variance (ANOVA) followed by a Bonferroni post hoc test was used. Statistical significance was set at $p < 0.05$.

SUPPLEMENTAL INFORMATION

Supplemental Information can be found online at https://doi.org/10.1016/j.omtm.2020.09.012.

AUTHOR CONTRIBUTIONS

M.W., H.K., and T.O. designed and conducted the research; M.W., Y.S., S.I., N.I., H.H., T.T., K.M., M.S., S.A., T.I., T.N., and H.K performed the research and analyzed the data; M.W. wrote the manuscript; H.K., K.M., M.S., H.I, and T.O. discussed the data and edited the manuscript.

CONFLICTS OF INTEREST

The authors declare no competing interests.

ACKNOWLEDGMENTS

This work was supported by a Grant-in-Aid for Scientific Research (grant no. 26461533) and was partially supported by the Practical Research Project for Rare/Intractable Diseases from the Japan Agency for Medical Research and Development (AMED; grant no. 19ek0109224h003). The authors are indebted to Joseph Muenzer (UNC Health Care) for providing MPS II mice and to Donald B. Kohn (UCLA) for providing the lentiviral vector. The authors also thank Yuki Asano (The Jikei University School of Medicine) for excellent technical assistance and the members of the Laboratory Animal Facility (The Jikei University School of Medicine) for assistance with the animal studies.

REFERENCES

1. Morishita, K., and Petty, R.E. (2011). Musculoskeletal manifestations of mucopolysaccharidoses. Rheumatology (Oxford) *50* (*Suppl 5*), v19–v25.
2. White, K.K. (2011). Orthopaedic aspects of mucopolysaccharidoses. Rheumatology (Oxford) *50* (*Suppl 5*), v26–v33.
3. Melbouci, M., Mason, R.W., Suzuki, Y., Fukao, T., Orii, T., and Tomatsu, S. (2018). Growth impairment in mucopolysaccharidoses. Mol. Genet. Metab. *124*, 1–10.
4. Stevenson, D.A., and Steiner, R.D. (2013). Skeletal abnormalities in lysosomal storage diseases. Pediatr. Endocrinol. Rev. *10* (*Suppl 2*), 406–416.
5. Okuyama, T., Tanaka, A., Suzuki, Y., Ida, H., Tanaka, T., Cox, G.F., Eto, Y., and Orii, T. (2010). Japan Elaprase Treatment (JET) study: idursulfase enzyme replacement therapy in adult patients with attenuated Hunter syndrome (mucopolysaccharidosis II, MPS II). Mol. Genet. Metab. *99*, 18–25.
6. Muenzer, J., Beck, M., Eng, C.M., Giugliani, R., Harmatz, P., Martin, R., Ramaswami, U., Vellodi, A., Wraith, J.E., Cleary, M., et al. (2011). Long-term, open-labeled extension study of idursulfase in the treatment of Hunter syndrome. Genet. Med. *13*, 95–101.
7. Muenzer, J., Wraith, J.E., Beck, M., Giugliani, R., Harmatz, P., Eng, C.M., Vellodi, A., Martin, R., Ramaswami, U., Gucsavas-Calikoglu, M., et al. (2006). A phase II/III clinical study of enzyme replacement therapy with idursulfase in mucopolysaccharidosis II (Hunter syndrome). Genet. Med. *8*, 465–473.
8. Al Sawaf, S., Mayatepek, E., and Hoffmann, B. (2008). Neurological findings in Hunter disease: pathology and possible therapeutic effects reviewed. J. Inherit. Metab. Dis. *31*, 473–480.
9. Manara, R., Priante, E., Grimaldi, M., Santoro, L., Astarita, L., Barone, R., Concolino, D., Di Rocco, M., Donati, M.A., Fecarotta, S., et al. (2011). Brain and spine MRI features of Hunter disease: frequency, natural evolution and response to therapy. J. Inherit. Metab. Dis. *34*, 763–780.
10. Wraith, J.E., Scarpa, M., Beck, M., Bodamer, O.A., De Meirleir, L., Guffon, N., Meldgaard Lund, A., Malm, G., Van der Ploeg, A.T., and Zeman, J. (2008). Mucopolysaccharidosis type II (Hunter syndrome): a clinical review and recommendations for treatment in the era of enzyme replacement therapy. Eur. J. Pediatr. *167*, 267–277.
11. Sato, Y., Fujiwara, M., Kobayashi, H., and Ida, H. (2013). Massive accumulation of glycosaminoglycans in the aortic valve of a patient with Hunter syndrome during enzyme replacement therapy. Pediatr. Cardiol. *34*, 2077–2079.
12. Sano, R., Tessitore, A., Ingrassia, A., and d'Azzo, A. (2005). Chemokine-induced recruitment of genetically modified bone marrow cells into the CNS of GM1-gangliosidosis mice corrects neuronal pathology. Blood *106*, 2259–2268.

13. Giugliani, R., Harmatz, P., Jones, S.A., Mendelsohn, N.J., Vellodi, A., Qiu, Y., Hendriksz, C.J., Vijayaraghavan, S., Whiteman, D.A., and Pano, A. (2017). Evaluation of impact of anti-idursulfase antibodies during long-term idursulfase enzyme replacement therapy in mucopolysaccharidosis II patients. Mol. Genet. Metab. Rep. *12*, 2–7.

14. Shapiro, E.G., Lockman, L.A., Balthazor, M., and Krivit, W. (1995). Neuropsychological outcomes of several storage diseases with and without bone marrow transplantation. J. Inherit. Metab. Dis. *18*, 413–429.

15. McKinnis, E.J., Sulzbacher, S., Rutledge, J.C., Sanders, J., and Scott, C.R. (1996). Bone marrow transplantation in Hunter syndrome. J. Pediatr. *129*, 145–148.

16. Vellodi, A., Young, E., Cooper, A., Lidchi, V., Winchester, B., and Wraith, J.E. (1999). Long-term follow-up following bone marrow transplantation for Hunter disease. J. Inherit. Metab. Dis. *22*, 638–648.

17. Guffon, N., Bertrand, Y., Forest, I., Fouilhoux, A., and Froissart, R. (2009). Bone marrow transplantation in children with Hunter syndrome: outcome after 7 to 17 years. J. Pediatr. *154*, 733–737.

18. Akiyama, K., Shimada, Y., Higuchi, T., Ohtsu, M., Nakauchi, H., Kobayashi, H., Fukuda, T., Ida, H., Eto, Y., Crawford, B.E., et al. (2014). Enzyme augmentation therapy enhances the therapeutic efficacy of bone marrow transplantation in mucopolysaccharidosis type II mice. Mol. Genet. Metab. *111*, 139–146.

19. Cartier, N., Hacein-Bey-Abina, S., Bartholomae, C.C., Veres, G., Schmidt, M., Kutschera, I., Vidaud, M., Abel, U., Dal-Cortivo, L., Caccavelli, L., et al. (2009). Hematopoietic stem cell gene therapy with a lentiviral vector in X-linked adrenoleukodystrophy. Science *326*, 818–823.

20. Biffi, A., Montini, E., Lorioli, L., Cesani, M., Fumagalli, F., Plati, T., Baldoli, C., Martino, S., Calabria, A., Canale, S., et al. (2013). Lentiviral hematopoietic stem cell gene therapy benefits metachromatic leukodystrophy. Science *341*, 1233158.

21. Aiuti, A., Biasco, L., Scaramuzza, S., Ferrua, F., Cicalese, M.P., Baricordi, C., Dionisio, F., Calabria, A., Giannelli, S., Castiello, M.C., et al. (2013). Lentiviral hematopoietic stem cell gene therapy in patients with Wiskott-Aldrich syndrome. Science *341*, 1233151.

22. Drakopoulou, E., Papanikolaou, E., and Anagnou, N.P. (2011). The ongoing challenge of hematopoietic stem cell-based gene therapy for β-thalassemia. Stem Cells Int. *2011*, 987980.

23. Visigalli, I., Delai, S., Politi, L.S., Di Domenico, C., Cerri, F., Mrak, E., D'Isa, R., Ungaro, D., Stok, M., Sanvito, F., et al. (2010). Gene therapy augments the efficacy of hematopoietic cell transplantation and fully corrects mucopolysaccharidosis type I phenotype in the mouse model. Blood *116*, 5130–5139.

24. Langford-Smith, A., Wilkinson, F.L., Langford-Smith, K.J., Holley, R.J., Sergijenko, A., Howe, S.J., Bennett, W.R., Jones, S.A., Wraith, J., Merry, C.L., et al. (2012). Hematopoietic stem cell and gene therapy corrects primary neuropathology and behavior in mucopolysaccharidosis IIIA mice. Mol. Ther. *20*, 1610–1621.

25. Wakabayashi, T., Shimada, Y., Akiyama, K., Higuchi, T., Fukuda, T., Kobayashi, H., Eto, Y., Ida, H., and Ohashi, T. (2015). Hematopoietic stem cell gene therapy corrects neuropathic phenotype in murine model of mucopolysaccharidosis type II. Hum. Gene Ther. *26*, 357–366.

26. Rowan, D.J., Tomatsu, S., Grubb, J.H., Montaño, A.M., and Sly, W.S. (2013). Assessment of bone dysplasia by micro-CT and glycosaminoglycan levels in mouse models for mucopolysaccharidosis type I, IIIA, IVA, and VII. J. Inherit. Metab. Dis. *36*, 235–246.

27. Kuehn, S.C., Koehne, T., Cornils, K., Markmann, S., Riedel, C., Pestka, J.M., Schweizer, M., Baldauf, C., Yorgan, T.A., Krause, M., et al. (2015). Impaired bone remodeling and its correction by combination therapy in a mouse model of mucopolysaccharidosis-I. Hum. Mol. Genet. *24*, 7075–7086.

28. Pievani, A., Azario, I., Antolini, L., Shimada, T., Patel, P., Remoli, C., Rambaldi, B., Valsecchi, M.G., Riminucci, M., Biondi, A., et al. (2015). Neonatal bone marrow transplantation prevents bone pathology in a mouse model of mucopolysaccharidosis type I. Blood *125*, 1662–1671.

29. Derrick-Roberts, A.L., Panir, K., Pyragius, C.E., Zarrinkalam, K.H., Atkins, G.J., and Byers, S. (2016). Reversal of established bone pathology in MPS VII mice following lentiviral-mediated gene therapy. Mol. Genet. Metab. *119*, 249–257.

30. Garcia, A.R., Pan, J., Lamsa, J.C., and Muenzer, J. (2007). The characterization of a murine model of mucopolysaccharidosis II (Hunter syndrome). J. Inherit. Metab. Dis. *30*, 924–934.

31. Cardone, M., Polito, V.A., Pepe, S., Mann, L., D'Azzo, A., Auricchio, A., Ballabio, A., and Cosma, M.P. (2006). Correction of Hunter syndrome in the MPSII mouse model by AAV2/8-mediated gene delivery. Hum. Mol. Genet. *15*, 1225–1236.

32. Gleitz, H.F., O'Leary, C., Holley, R.J., and Bigger, B.W. (2017). Identification of age-dependent motor and neuropsychological behavioural abnormalities in a mouse model of mucopolysaccharidosis type II. PLoS ONE *12*, e0172435.

33. Polito, V.A., and Cosma, M.P. (2009). IDS crossing of the blood-brain barrier corrects CNS defects in MPSII mice. Am. J. Hum. Genet. *85*, 296–301.

34. Gleitz, H.F., Liao, A.Y., Cook, J.R., Rowlston, S.F., Forte, G.M., D'Souza, Z., O'Leary, C., Holley, R.J., and Bigger, B.W. (2018). Brain-targeted stem cell gene therapy corrects mucopolysaccharidosis type II via multiple mechanisms. EMBO Mol. Med. *10*, e8730.

35. Motas, S., Haurigot, V., Garcia, M., Marcó, S., Ribera, A., Roca, C., Sánchez, X., Sánchez, V., Molas, M., Bertolin, J., et al. (2016). CNS-directed gene therapy for the treatment of neurologic and somatic mucopolysaccharidosis type II (Hunter syndrome). JCI Insight *1*, e86696.

36. Derrick-Roberts, A.L., Pyragius, C.E., Kaidonis, X.M., Jackson, M.R., Anson, D.S., and Byers, S. (2014). Lentiviral-mediated gene therapy results in sustained expression of β-glucuronidase for up to 12 months in the $Gus^{mps/mps}$ and up to 18 months in the $Gus^{tm(L175F)Sly}$ mouse models of mucopolysaccharidosis type VII. Hum. Gene Ther. *25*, 798–810.

37. Macsai, C.E., Derrick-Roberts, A.L., Ding, X., Zarrinkalam, K.H., McIntyre, C., Anderson, P.H., Anson, D.S., and Byers, S. (2012). Skeletal response to lentiviral mediated gene therapy in a mouse model of MPS VII. Mol. Genet. Metab. *106*, 202–213.

38. Salbach-Hirsch, J., Kraemer, J., Rauner, M., Samsonov, S.A., Pisabarro, M.T., Moeller, S., Schnabelrauch, M., Scharnweber, D., Hofbauer, L.C., and Hintze, V. (2013). The promotion of osteoclastogenesis by sulfated hyaluronan through interference with osteoprotegerin and receptor activator of NF-κB ligand/osteoprotegerin complex formation. Biomaterials *34*, 7653–7661.

39. Martin, T.J. (2013). Historically significant events in the discovery of RANK/RANKL/OPG. World J. Orthop. *4*, 186–197.

40. Maeda, K., Takahashi, N., and Kobayashi, Y. (2013). Roles of Wnt signals in bone resorption during physiological and pathological states. J. Mol. Med. (Berl.) *91*, 15–23.

41. Dumas, A., Brigitte, M., Moreau, M.F., Chrétien, F., Baslé, M.F., and Chappard, D. (2009). Bone mass and microarchitecture of irradiated and bone marrow-transplanted mice: influences of the donor strain. Osteoporos. Int. *20*, 435–443.

42. Wright, L.E., Buijs, J.T., Kim, H.S., Coats, L.E., Scheidler, A.M., John, S.K., She, Y., Murthy, S., Ma, N., Chin-Sinex, H.J., et al. (2015). Single-limb irradiation induces local and systemic bone loss in a murine model. J. Bone Miner. Res. *30*, 1268–1279.

43. Shiraishi, A., Miyabe, S., Nakano, T., Umakoshi, Y., Ito, M., and Mihara, M. (2009). The combination therapy with alfacalcidol and risedronate improves the mechanical property in lumbar spine by affecting the material properties in an ovariectomized rat model of osteoporosis. BMC Musculoskelet. Disord. *10*, 66.

44. Nakano, T., Kaibara, K., Tabata, Y., Nagata, N., Enomoto, S., Marukawa, E., and Umakoshi, Y. (2002). Unique alignment and texture of biological apatite crystallites in typical calcified tissues analyzed by microbeam X-ray diffractometer system. Bone *31*, 479–487.

45. Saito, M., and Marumo, K. (2010). Collagen cross-links as a determinant of bone quality: a possible explanation for bone fragility in aging, osteoporosis, and diabetes mellitus. Osteoporos. Int. *21*, 195–214.

46. Seeman, E., and Delmas, P.D. (2006). Bone quality—the material and structural basis of bone strength and fragility. N. Engl. J. Med. *354*, 2250–2261.

47. NIH Consensus Development Panel on Osteoporosis Prevention, Diagnosis, and Therapy (2001). Osteoporosis prevention, diagnosis, and therapy. JAMA *285*, 785–795.

48. Kobayashi, H., Carbonaro, D., Pepper, K., Petersen, D., Ge, S., Jackson, H., Shimada, H., Moats, R., and Kohn, D.B. (2005). Neonatal gene therapy of MPS I mice by intravenous injection of a lentiviral vector. Mol. Ther. *11*, 776–789.

49. Falahati, R., Zhang, J., Flebbe-Rehwaldt, L., Shi, Y., Gerson, S.L., and Gaensler, K.M. (2012). Chemoselection of allogeneic HSC after murine neonatal transplantation without myeloablation or post-transplant immunosuppression. Mol. Ther. *20*, 2180–2189.

50. Higuchi, T., Shimizu, H., Fukuda, T., Kawagoe, S., Matsumoto, J., Shimada, Y., Kobayashi, H., Ida, H., Ohashi, T., Morimoto, H., et al. (2012). Enzyme replacement therapy (ERT) procedure for mucopolysaccharidosis type II (MPS II) by intraventricular administration (IVA) in murine MPS II. Mol. Genet. Metab. *107*, 122–128.

51. Shimada, Y., Wakabayashi, T., Akiyama, K., Hoshina, H., Higuchi, T., Kobayashi, H., Eto, Y., Ida, H., and Ohashi, T. (2016). A method for measuring disease-specific iduronic acid from the non-reducing end of glycosaminoglycan in mucopolysaccharidosis type II mice. Mol. Genet. Metab. *117*, 140–143.

52. Hoshina, H., Shimada, Y., Higuchi, T., Kobayashi, H., Ida, H., and Ohashi, T. (2018). Chaperone effect of sulfated disaccharide from heparin on mutant iduronate-2-sulfatase in mucopolysaccharidosis type II. Mol. Genet. Metab. *123*, 118–122.

53. Ohashi, T., Iizuka, S., Shimada, Y., Higuchi, T., Eto, Y., Ida, H., and Kobayashi, H. (2012). Administration of anti-CD3 antibodies modulates the immune response to an infusion of α-glucosidase in mice. Mol. Ther. *20*, 1924–1931.

54. Kimura, T., Koya, R.C., Anselmi, L., Sternini, C., Wang, H.J., Comin-Anduix, B., Prins, R.M., Faure-Kumar, E., Rozengurt, N., Cui, Y., et al. (2007). Lentiviral vectors with CMV or MHCII promoters administered in vivo: immune reactivity versus persistence of expression. Mol. Ther. *15*, 1390–1399.

55. Elliger, S.S., Elliger, C.A., Lang, C., and Watson, G.L. (2002). Enhanced secretion and uptake of β-glucuronidase improves adeno-associated viral-mediated gene therapy of mucopolysaccharidosis type VII mice. Mol. Ther. *5*, 617–626.

56. Parfitt, A.M., Drezner, M.K., Glorieux, F.H., Kanis, J.A., Malluche, H., Meunier, P.J., Ott, S.M., and Recker, R.R. (1987). Bone histomorphometry: standardization of nomenclature, symbols, and units. Report of the ASBMR Histomorphometry Nomenclature Committee. J. Bone Miner. Res. *2*, 595–610.

57. Saito, M., Marumo, K., Soshi, S., Kida, Y., Ushiku, C., and Shinohara, A. (2010). Raloxifene ameliorates detrimental enzymatic and nonenzymatic collagen cross-links and bone strength in rabbits with hyperhomocysteinemia. Osteoporos. Int. *21*, 655–666.

58. Jämsä, T., Jalovaara, P., Peng, Z., Väänänen, H.K., and Tuukkanen, J. (1998). Comparison of three-point bending test and peripheral quantitative computed tomography analysis in the evaluation of the strength of mouse femur and tibia. Bone *23*, 155–161.

59. Ishimoto, T., Sato, B., Lee, J.W., and Nakano, T. (2017). Co-deteriorations of anisotropic extracellular matrix arrangement and intrinsic mechanical property in c-*src* deficient osteopetrotic mouse femur. Bone *103*, 216–223.

OMTM, Volume *19*

Supplemental Information

Ex Vivo Gene Therapy Treats Bone Complications of Mucopolysaccharidosis Type II Mouse Models through Bone Remodeling Reactivation

Miho Wada, Yohta Shimada, Sayoko Iizuka, Natsumi Ishii, Hiromi Hiraki, Toshiaki Tachibana, Kazuhiro Maeda, Mitsuru Saito, Shoutaro Arakawa, Takuya Ishimoto, Takayoshi Nakano, Hiroyuki Ida, Toya Ohashi, and Hiroshi Kobayashi

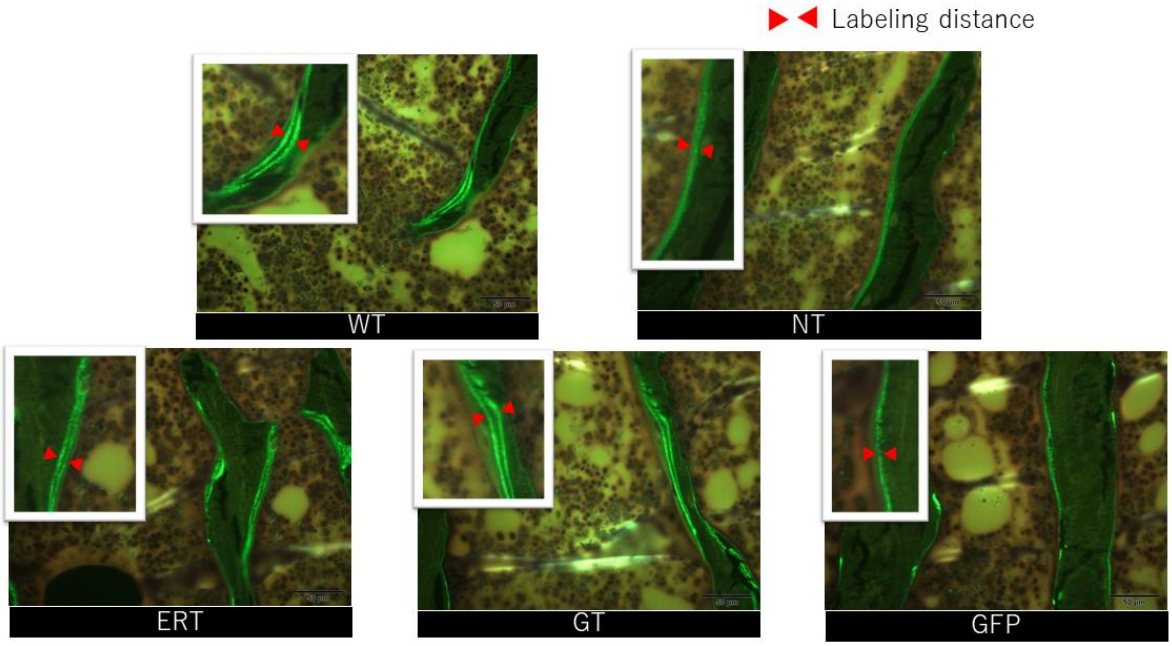

Figure S1. Fluorescence of the tibia

Histopathological results obtained from WT, NT, ERT, GT, and *eGFP* mice 12 weeks after initiating treatments. Using a fluorescence microscope, we observed the images of fluorescently labeled calcein. The width between the two red triangles represents the length of bone formation during the calcein dosing interval (4 days). The distance between two fluorescently labeled calcification fronts was measured with a fluorescence microscope to determine how much bone was formed during this interval. This distance was longer in ERT mice and even GT mice than in NT mice.

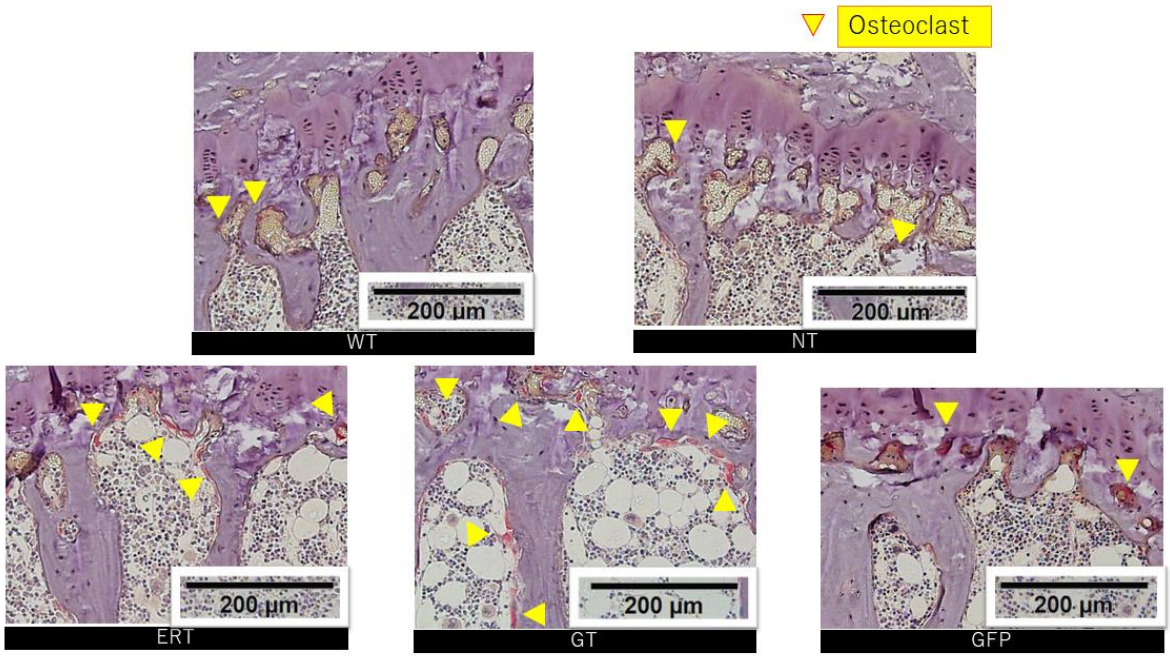

Figure S2. TRAP staining of the tibia

Tartrate-resistant acid phosphatase (TRAP) staining of the tibia from WT, NT, ERT, GT, and *eGFP* mice 12 weeks after initiating treatments. Yellow triangles in the images indicate osteoclasts as pinkish region with TRAP staining. More osteoclasts were observed in GT mice than in NT mice.

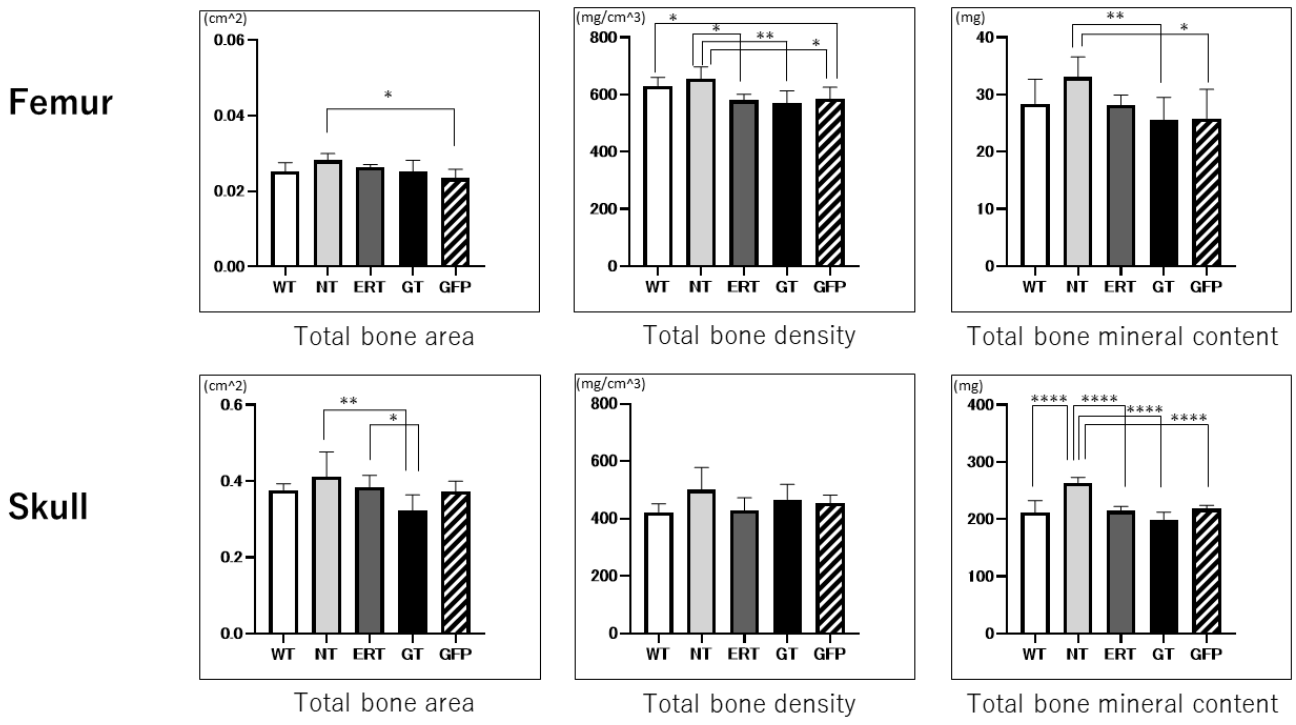

Figure S3. Micro CT value analysis

Micro CT value analysis of skull and femur obtained from WT, NT, ERT, GT, and *eGFP* mice 12 weeks after initiating treatments. The total bone surface, total bone mineral density, and total bone mineral content were measured using micro CT scan (mean ± SD, n = 5–10). Total bone surface in the skull of GT mice was significantly lower than that in the skull of NT and ERT mice. Total bone mineral density in the femur of ERT and GT mice was significantly lower than that in the femur of NT mice. Total bone mineral content in the femur of GT mice was significantly lower than that in the femur of NT mice. Statistical analyses of the data were performed by one-way analysis of variance (post-test; Bonferroni) *(*$p < 0.05$, **$p < 0.01$, ****$p < 0.0001$).*